Research Square

Preprints are preliminary reports that have not undergone peer review.
They should not be considered conclusive, used to inform clinical practice,
or referenced by the media as validated information.

Rising natural aerosols drive marine radiative forcing as pollution declines

Vaios Moschos

vaios.moschos@universityofgalway.ie

University of Galway https://orcid.org/0000-0002-6251-4117

Emmanuel Chevassus

University Of Galway

Kirsten Fossum

University of Galway https://orcid.org/0000-0002-4976-7259

Lu Lei

University of Galway

Jakob Pernov

Queensland University of Technology

Ruhi Humphries

CSIRO https://orcid.org/0000-0002-4864-5321

Melita Keywood

CSIRO Ocean and Atmosphere Flagship

Colin O'Dowd

National University of Ireland Galway https://orcid.org/0000-0002-3068-2212

Darius Ceburnis

University Of Galway

Jurgita Ovadnevaite

University Of Galway https://orcid.org/0000-0001-7201-0118

Physical Sciences - Article

Keywords:

Posted Date: March 4th, 2026

DOI: https://doi.org/10.21203/rs.3.rs-8776460/v1

License: This work is licensed under a Creative Commons Attribution 4.0 International License.
Read Full License

Additional Declarations: There is **NO** Competing Interest.

Rising natural aerosols drive marine radiative forcing as pollution declines

Vaios Moschos[†*], Emmanuel Chevassus[†], Kirsten N. Fossum[†], Lu Lei[†], Jakob B. Pernov[§], Ruhi S. Humphries[⊥], Melita D. Keywood[⊥], Colin O'Dowd[†], Darius Ceburnis[†], and Jurgita Ovadnevaite[†*]

[†] School of Natural Sciences, Ryan Institute's Centre for Climate and Air Pollution Studies, University of Galway, Galway, Ireland

[§] School of Earth and Atmospheric Sciences, Queensland University of Technology, Brisbane, Australia

[⊥] Environment Research Unit, Commonwealth Scientific and Industrial Research Organisation (CSIRO), Melbourne, Victoria, Australia

* Corresponding Authors:

Vaios Moschos; vaios.moschos@universityofgalway.ie

Jurgita Ovadnevaite; jurgita.ovadnevaite@universityofgalway.ie

Abstract

Atmospheric aerosol particles are the leading uncertainty in climate forcing because they both reflect and absorb sunlight. Over the oceans, this influence is poorly constrained because long-term, composition-resolved observations are rare and natural sources vary widely. Using 2008–2019 aerosol records from interhemispheric observatories at Mace Head (Ireland) and Kennaook/Cape Grim (Tasmania), we show that increasing natural aerosol concentrations are driving increasingly negative marine aerosol forcing. After removing seasonality and quantifying trends across the concentration distribution, we find that at Mace Head historical declines in ammonium-sulfate and combustion-derived organics have largely levelled off, and the net anthropogenic forcing trend is now indistinguishable from zero because reduced scattering is offset by weaker black/brown carbon absorption. By contrast, increases in sea-salt, biogenic sulfate and marine organics drive a robust cooling trend (median −0.03 W m^{-2} $decade^{-1}$; −0.05 W m^{-2} $decade^{-1}$ at background levels). At Kennaook/Cape Grim, decreasing black carbon alongside increasing biogenic sulfate indicates that this shift is not confined to the North Atlantic. Meanwhile, extreme aerosol episodes linked to wildfire smoke, marine blooms and long-range transport also increase. These results show that evolving natural aerosol sources must be represented in climate models to correctly attribute and project near-term marine forcing.

Main

Near-term climate forcing remains uncertain because atmospheric aerosol concentrations—and their radiative effects—respond rapidly to evolving natural and anthropogenic emissions.[1,2] In coastal environments, strong variability in aerosol sources and composition can produce radiative forcing perturbations that are regionally substantial and, at times, comparable to greenhouse-gas forcing.[3,4] Yet long-term, composition-resolved aerosol records are rare: few observatories separate marine from pollution sources, and most are in the Northern Hemisphere.[5-7] Satellite

observations provide global coverage[8] but poorly constrain near-surface mass and composition,[9] so trend attribution still relies on sparse in situ measurements and uncertain model hindcasts.[10]

Detecting long-term aerosol trends is further complicated by strong seasonality, skewed distributions, and episodic extremes.[11,12] Analyses focused on central tendency can miss baseline shifts and changes in the upper tail, where climate-relevant signals can emerge.[13] Here we isolate long-term change from seasonality and quantify trends across the concentration distribution (background to extremes). Combining Seasonal–Trend decomposition via Loess (STL)[14] with quantile regression (QR),[15] we estimate trends in a decade-long, chemically resolved aerosol record from the Mace Head marine observatory, Ireland (MHD),[16,17] and compare key indicators with an equivalent record from Kennaook/Cape Grim, Tasmania (CGO).

We first analyse 2008–2019 submicron particulate matter (PM_1; particles smaller than 1 μm) at MHD (Methods). Using chemical measurements and source apportionment (Methods; Text S1–S2; Figs. S1–S2), we separate pollution-dominated aerosol (including black carbon, nitrate, sulfate and combustion organics) from marine/biogenic aerosol (including sea-salt, dimethyl-sulfide-derived sulfur species and marine organics). We then convert observed mass trends into all-sky direct radiative forcing trends and assess whether similar changes occur at CGO (in the opposite hemisphere) using long-term measurements of black carbon and biogenic sulfur tracers.

At MHD, anthropogenic components peak in late winter and spring (Fig. 1a–f), with the highest monthly concentrations (Fig. 1g) observed for ammonium-sulfate (AS_a) and ammonium-nitrate (AN). Natural (marine) aerosols peak from late spring through summer, except for sea-salt (SS), which is enhanced during winter storms and high winds (Fig. 1h–m); the highest monthly concentrations (Fig. 1n) are observed for SS and primary marine organic-aerosol (PMOA). These distinct seasonal cycles indicate that combustion sources dominate during colder months, whereas marine processes dominate during warmer months.

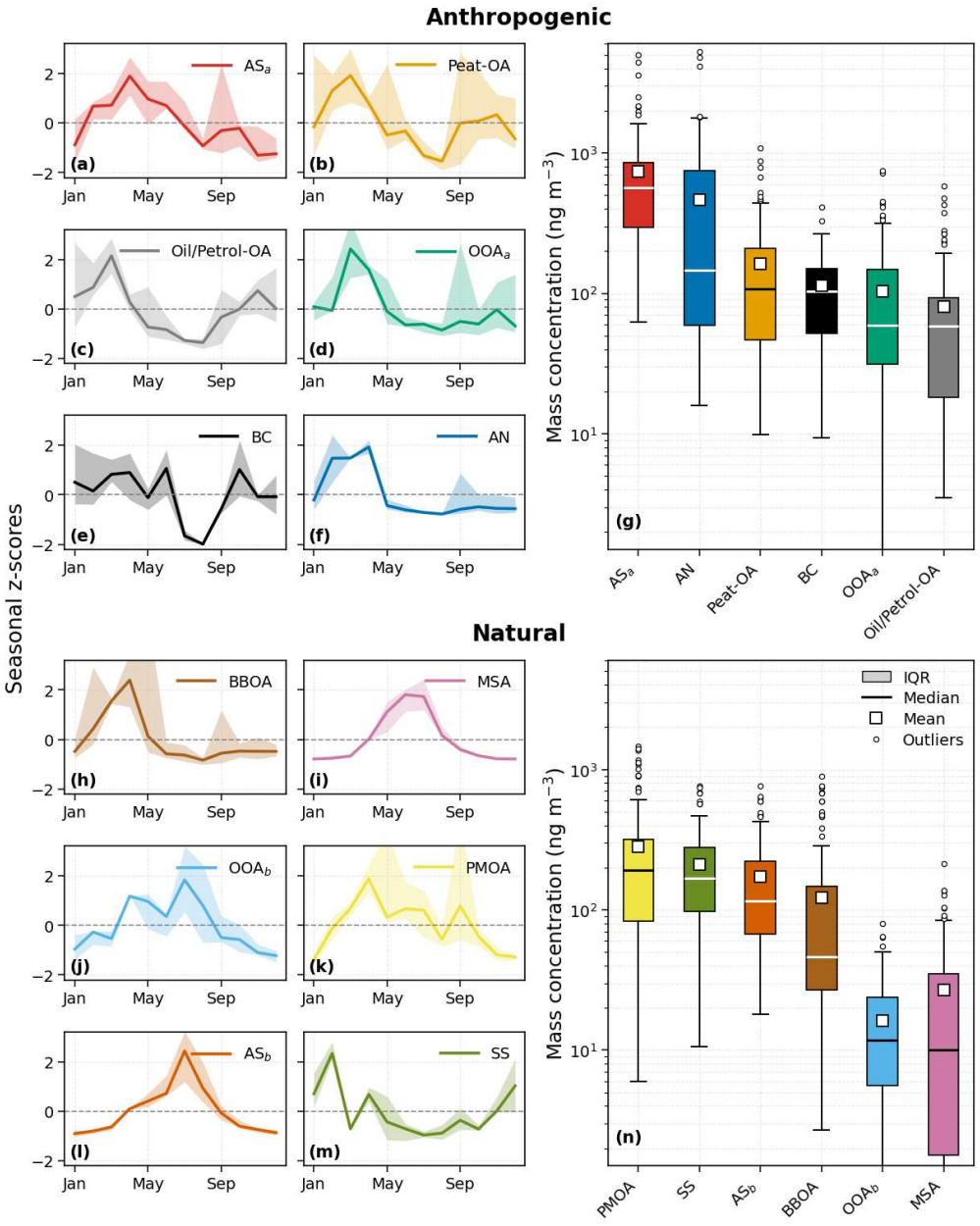


Figure 1. Seasonal patterns and mass concentrations of aerosol components at MHD based on monthly data from 2008–2019. Panels (a–f) show the standardised annual cycle (monthly z-scores; shaded areas: interquartile range, IQR) for the anthropogenic components (ammonium-sulfate, AS_a; peat-combustion organic-aerosol, Peat-OA; Oil/Petrol-OA; oxygenated organic-aerosol, OOA_a; black carbon, BC; and ammonium-nitrate, AN). Panel (g) shows the corresponding monthly mass-concentration boxplots for anthropogenic components (126 monthly values per component; components sorted by median); whiskers denote values within 1.5×IQR of the quartiles. Panels (h–m) show the monthly z-scores for the natural components (biomass-burning OA, BBOA; methane-sulphonic acid, MSA; oxygenated OA, OOA_b; primary marine organic-aerosol, PMOA; ammonium-sulfate, AS_b; and sea-salt, SS). Panel (n) shows the corresponding monthly mass-concentration boxplots for natural components. Z-scores were obtained by taking, for each calendar month, the median across years (robust to extreme values) and then standardising the resulting 12 monthly medians using their mean and standard deviation. Figure S2 shows the decadal evolution of yearly mean speciated PM_1 and OA.

To quantify changes across the concentration distribution, we first use STL to isolate a low-frequency, nonlinear trend component (STL Trend) from seasonality and residual variability (Fig. S3). Figure 2 shows contrasting low-frequency behaviour: over the decade, anthropogenic components decline (Fig. 2a), whereas natural components increase (Fig. 2b). We then apply QR to the STL Trends to estimate slopes across quantiles (Methods; Text S3; Fig. S3), capturing changes in background conditions, central tendency and the upper tail.

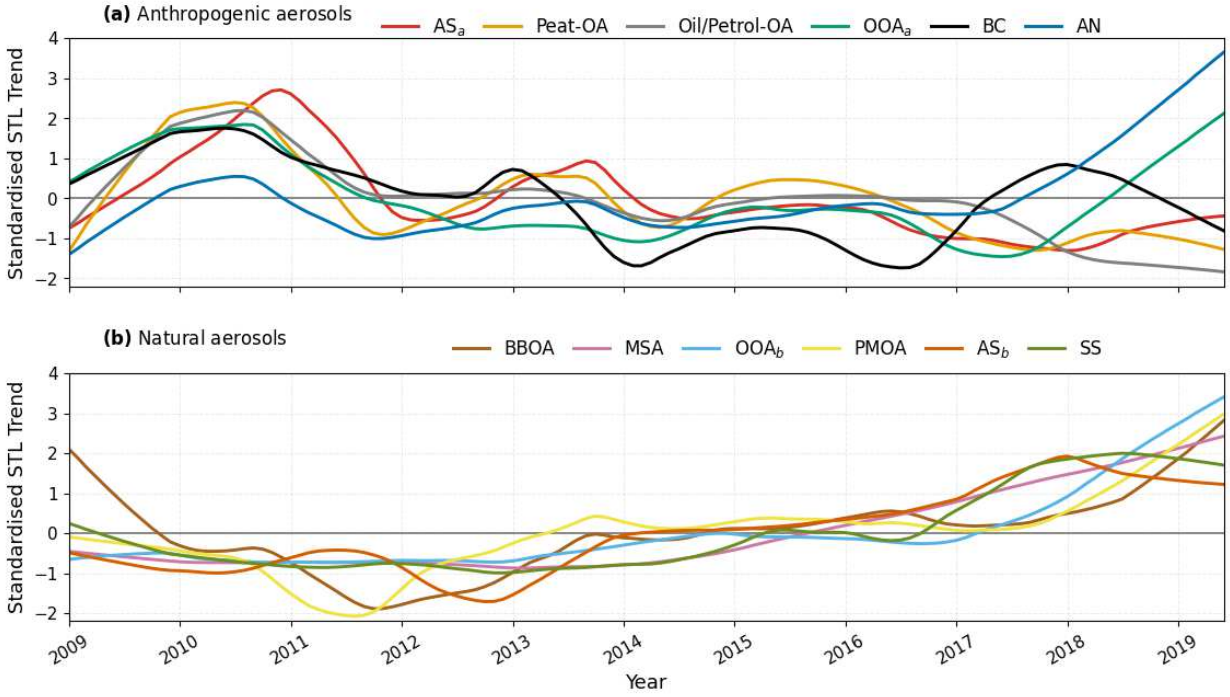


Figure 2. Standardised STL Trend components of the MHD time series (dimensionless z-scores; derived from panels (b) of Fig. S3), illustrating the non-linear decadal evolution of anthropogenic (a) and natural/biogenic (b) aerosol components after removing seasonal-cycle variability and outlier-driven variability from the original monthly series (see Methods). Lines connect monthly STL Trend estimates (12 points per year; no further smoothing was applied). See Fig. S3 for the full component-specific STL decomposition outputs.

Divergent anthropogenic–natural aerosol trends

Figure 3a summarizes the absolute QR slopes (ng m^{-3} yr^{-1}) at τ=0.25, 0.50 and 0.75 representing the lower, median and upper parts of the distribution, respectively. Relative slopes (% yr^{-1}; Figs. S4–S5) are normalised to each component's baseline to facilitate comparison across species and sites. QR and Theil–Sen applied to the STL Trends yield consistent median slopes, whereas

estimates from non-deseasonalized time series are more sensitive to seasonality and high-frequency variability (Fig. S6), supporting the robustness of the STL–QR framework.

Most anthropogenic components decline across quantiles (Fig. 3a). The steepest decline is observed for AS_a (–13 to –23 ng m^{-3} yr^{-1}; –2 to –4% yr^{-1}), consistent with European SO_2 and NH_3 emission reductions;[18] this may also include contributions from reduced shipping SO_2 after the 2015 North Sea/Baltic SECA fuel-sulphur tightening (0.10%) and earlier global sulfur caps.[19] Combustion-related OAs (Oil/Petrol-OA; Peat-OA) decrease by –4 to –10 ng m^{-3} yr^{-1} (–4 to –9% yr^{-1}), especially at higher quantiles (Figs. S4-S5), reflecting mitigation of residential heating emissions (solid fuels and heating oil) in parts of Europe, including Ireland.[20] Anthropogenic oxygenated organic-aerosol (OOA_a) and black carbon (BC) also decline, with larger negative slopes at τ=0.25 than at higher quantiles (Fig. 3a), suggesting that baseline concentrations are decreasing more rapidly than upper-tail events. AN shows a positive slope, likely reflecting shifting partitioning as declining sulfate frees NH_3 to form NH_4NO_3; AN therefore reflects coupled NO_x–NH_3–SO_2 chemistry and transport rather than NO_x emissions alone.[21-24]

In contrast, all natural aerosol components exhibit significant upward trends (Fig. 3a), with QR 95% confidence intervals excluding zero across the reported quantiles. For most natural components, the strongest increases occur at τ=0.25 (except OOA_b; Fig. S5), indicating rising background concentrations. SS increases by 8–13 ng m^{-3} (~6%) yr^{-1} across quantiles, consistent with wind-driven sea-salt emission sensitivity[25,26] and with a positive wind-speed trend at MHD over the study period (up to +1.5% yr^{-1} at τ=0.25). OOA_b, MSA, PMOA, and AS_b increase by 3–10% yr^{-1} (Fig. S5), suggesting enhanced marine aerosol and precursor emissions as well as the secondary formation. This pattern is consistent with independent reports of increasing chlorophyll-a in the North Atlantic,[27] which suggest enhanced marine biological activity. The climate-change-sensitive Arctic also experiences increases in natural/biogenic aerosol concentrations.[28] Together, these patterns point to climate-sensitive processes—including wind-driven sea–air

exchange and biogenic emissions—amplifying natural aerosol production, consistent with process-level studies linking sea-spray aerosol, marine biology and cloud-relevant particle populations.[26,29]

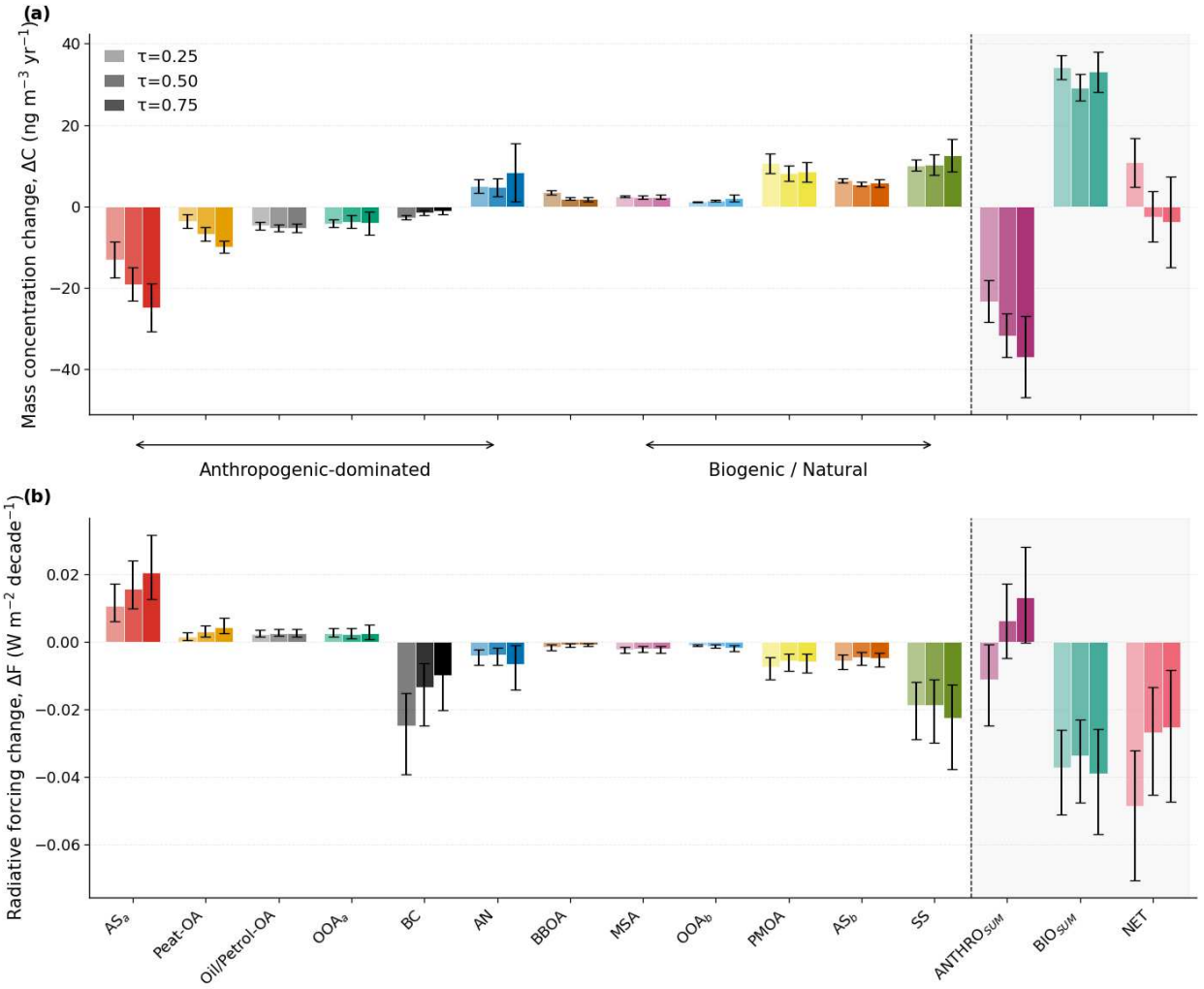


Figure 3. Trends in mass concentrations (a) and direct radiative forcing (b). Results from QR on the STL Trend of each aerosol component at MHD from 2008–2019: (a) Absolute trends in concentration (ng m^{-3} yr^{-1}). Trend slopes are shown for the 25th (τ=0.25), median (τ=0.50), and 75th (τ=0.75) percentiles (represented by different shades of colour) for each aerosol species to capture distributional variability, with error bars corresponding to 95% confidence intervals. Entire distributions are illustrated as tau-grid plots (Fig. S4). b) Corresponding changes in direct radiative forcing, shown as medians with 16th–84th percentile intervals from the Monte Carlo analysis.

Natural aerosols drive net cooling

Next, we estimate how the opposing trends in anthropogenic and natural aerosols affect direct radiative forcing (RF). Our Monte Carlo RF analysis (Methods; Text S4) samples component-

specific extinction/absorption efficiencies from observation-constrained, size-dependent ranges, yielding forcing distributions (Fig. S7) consistent with observations and robust to size uncertainty.

After decades of strong decline,[18] anthropogenic ammonium-sulfate, and combustion-derived primary and secondary organics (which include brown-carbon; Text S4), have levelled off but continue to decline at a lower rate (Fig. 3a). Despite this, the direct RF trend for the combined anthropogenic components is small and statistically indistinguishable from zero at τ=0.50 and τ=0.75 within the Monte Carlo uncertainty range (16^{th}–84^{th} percentiles). This is largely because the concurrent decline in BC reduces absorption (Fig. 3b), offseting the warming that would otherwise result from reduced scattering by AS_a and brown-carbon-containing OAs. For these OAs, the reduction in scattering dominates over the reduction in brown-carbon absorption (Fig. 3b). At τ=0.25, the BC decline exerts a stronger impact, yielding a negative RF change for the anthropogenic class (Fig. 3b).

By contrast, natural aerosol components at MHD—including marine biogenic sulfate, sea-salt, and primary/secondary marine OAs—exert a combined negative forcing over 2008–2019 of –0.04 W m^{-2} $decade^{-1}$. The natural class dominates the RF budget (Fig. 3b) and sets the sign of the total (net) direct aerosol forcing, which is negative across quantiles (around –0.03 W m^{-2} $decade^{-1}$) and becomes stronger at τ=0.25 (–0.05 W m^{-2} $decade^{-1}$). Overall, the net negative direct radiative effect at MHD is driven by enhanced scattering from rising natural aerosols, rather than by the radiative response to declining anthropogenic aerosol concentrations.

Figure 3b indicates a regime in which natural aerosols control both the magnitude and sign of the direct forcing trend, with anthropogenic changes now playing a secondary role. When estimating source contributions and RF trends, ignoring the observed rise in natural aerosols would bias attribution of the net forcing trend and could even lead to an incorrect inferred sign for the direct forcing adjustment.

We further apply STL–QR to air temperature (T) and sea surface temperature (SST) at MHD (2008–2019). Both increase across quantiles (T: 0.4–1.0 °C decade^{-1}; SST: 0.1–0.3 °C decade^{-1}), with the largest increases near the median, despite the net negative trend in direct aerosol RF. Rising SST could contribute to increasing SS through enhanced air–sea exchange,[29,30] although this linkage is not directly resolved here. Overall, while greenhouse-gas–driven warming dominates the energy balance, evolving aerosols can modulate the regional response.

Hemispheric consistency at Kennaook/Cape Grim

To test whether the anthropogenic–natural divergence observed at MHD is regionally specific, we compare STL–QR trends for key aerosol species (BC, MSA, biogenic nssSO_4) against those at Kennaook/Cape Grim (CGO) over 2008–2019 (Fig. 4). A full anthropogenic-versus-natural mass (and direct RF) balance is not calculated for CGO because only a subset of species is available at this site, preventing construction of summed anthropogenic and natural component totals.

BC trends at CGO broadly match those observed at MHD (Fig. 4), with decreases across all quantiles. At CGO, BC declines more moderately (to ~–2 ng m^{-3} yr^{-1} at high τ; Fig. 4a), whereas MHD shows larger decreases at low τ (–2 to –3 ng m^{-3} yr^{-1}) that weaken toward the upper tail. This cross-hemispheric coherence reflects ongoing reductions in fossil-fuel and biomass-combustion emissions delivered to both regions, despite the lower anthropogenic burden and generally weaker wildfire/biomass-burning influence in the Southern Hemisphere.[31]

Biogenic sulfate indicators increase at both sites. At MHD, MSA (Fig. 4c) and biogenic nssSO_4 (Fig. 4e) show persistent, positive trends that are largely insensitive to quantile, implying strengthened marine biogenic sulfur production across both baseline and moderate concentrations. At CGO, MSA shows clearer quantile dependence: increases are modest at low τ but reach ~1 ng m^{-3} yr^{-1} at τ ≈ 0.8. Relative trends exceed 2.5% yr^{-1} at the upper quantiles (Fig. 4d), consistent with an expansion of DMS-derived sulfate in the Southern Ocean region and potentially reflecting higher DMS emissions and/or more efficient conversion to MSA.

At MHD, $nssSO_4$ increases by ~4–6 ng m^{-3}, corresponding to ~2–4% yr^{-1} (Figs. 4e–f), whereas at CGO increases reach up to ~13 ng m^{-3} (~9% yr^{-1}). Together, the concurrent rise in MSA and biogenic $nssSO_4$ suggests increasing DMS emissions and/or higher total oxidant levels, rather than a shift in the dominant oxidation pathway.

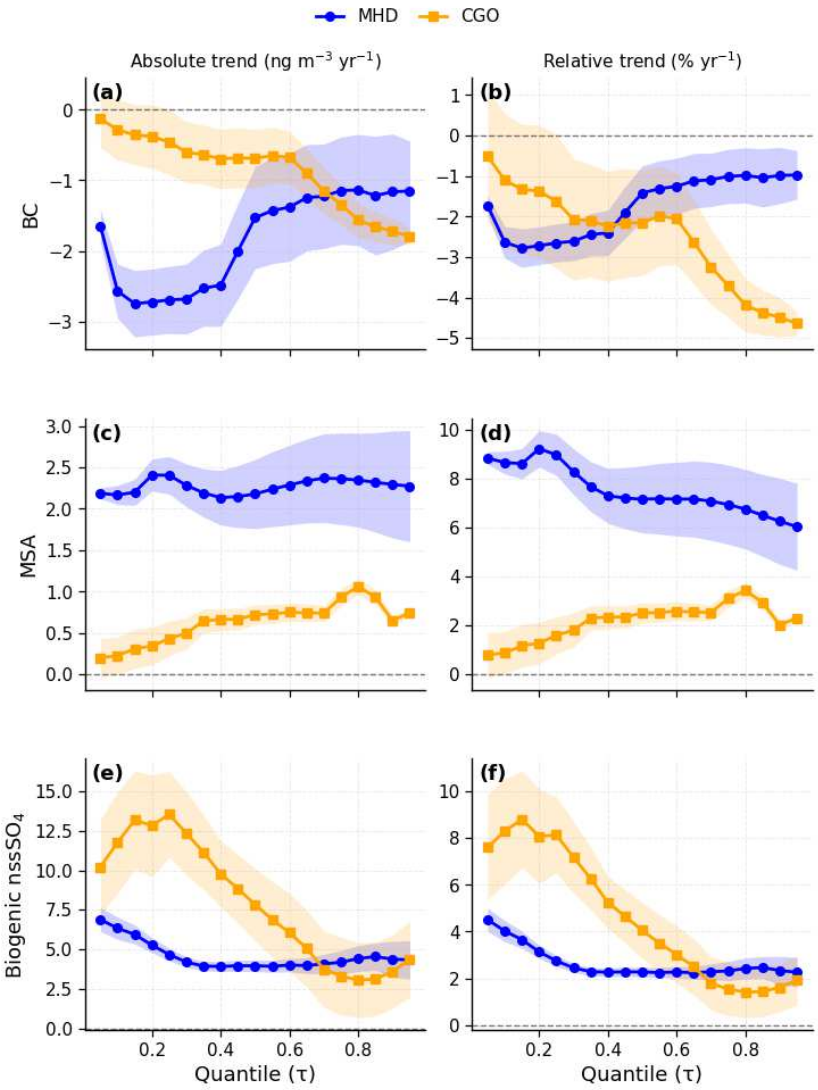


Figure 4. Quantile-resolved decadal trends in natural and anthropogenic aerosol indicators at Mace Head (MHD) and Kennaook/Cape Grim (CGO), 2008–2019. Absolute (left) and relative (right) QR trend slopes for STL Trends across quantiles (τ=0.05–0.95; i.e. tau-grid plots) for (a–b) black carbon, (c–d) MSA, and (e–f) biogenic non-sea-salt (nss) sulfate. Solid markers denote trend estimates for each quantile, with shaded envelopes representing 95% confidence intervals.

Satellite chlorophyll-a trends provide independent support for enhanced marine biogenic activity in air masses upwind of both sites. Chlorophyll-a is a proxy for phytoplankton productivity[32] and

can covary with DMS emissions, whose oxidation contributes to aerosol-phase nssSO_4 and MSA. Recent studies report increasing chlorophyll-a over the past 25 years in the North Atlantic Drift (upwind of Mace Head),[27] Subantarctic (upwind of KCG) provinces,[27] and the Southern Ocean,[33] consistent with the sign of the DMS-derived aerosol trends observed here.

Hemispheric agreement in trend direction implies that the anthropogenic–natural divergence is not region-specific, although its strength depends on regional biogeochemistry and meteorology. The coupled decline in anthropogenic markers and rise in biogenic indicators is consistent with a broader shift in marine boundary-layer aerosol regimes under declining anthropogenic (combustion) emissions and warming, increasingly productive oceans. Cross-site inference remains limited by chemical resolution and site-specific context, motivating high-resolution observations across diverse regions.

Intensifying extreme aerosol events

To isolate episodic departures from expected behaviour and assess trends in extreme events, we apply QR at τ=0.95 to STL Residuals and examine components at MHD with significant upward trends (Table S1). AN shows a strong increase in extreme concentrations, indicating that episodic high-AN events (e.g. Jan–Apr 2013, Oct 2015, Apr 2019) are intensifying relative to baseline, consistent with continental transport episodes previously shown to drive high nitrate/ammonium at MHD.[34,35] BBOA also exhibits growing episodic peaks (e.g. May 2010, Feb–Apr 2013, Jul 2018), consistent with an increase in reported gorse and grass fires in western Ireland uplands.[36] Whereas the mean BBOA diurnal cycle peaks at night (data not shown), extreme BBOA events show a flatter profile, implying an additional contribution from transported wildfire smoke on top of residential burning. Increasing τ=0.95 slopes therefore indicate a rising influence of episodic fire-related emissions on upper-tail BBOA variability. PMOA extremes intensify from spring to early autumn (e.g. Mar–Apr 2013, Oct 2015, Apr 2019), broadly coinciding with phytoplankton blooms and marine biological activity in the highly productive northeast Atlantic region. This

increase in PMOA extremes aligns with increases in natural aerosol components and supports enhanced marine biogenic activity and emissions.

Implications for future climate forcing

While pollution-derived aerosol mass continues to decline, increasing natural aerosol—especially at background conditions—now exerts greater control over the sign and magnitude of trends in direct radiative forcing in the marine boundary-layer. This pattern suggests a shift towards marine aerosol regimes in which climate-sensitive natural sources increasingly shape near-term forcing.[37]

A recent modelling study[38] estimated that aerosol emission reductions strengthened the 2001–2019 Earth energy-imbalance trend by 0.2 ± 0.1 W m^{-2} $decade^{-1}$ via aerosol effective RF. Our MHD record shows a smaller trend in direct aerosol–radiation forcing (Fig. 3b), consistent with focusing on the direct effect rather than full effective RF. Rising natural aerosol emissions—via sea–air exchange, marine productivity, chemical conversion, and storm/wind changes—can offset the warming expected from declining anthropogenic particles, so emissions trajectories alone are insufficient for predicting aerosol–radiation responses.[39,40]

The interhemispheric coherence suggests that strengthened natural aerosol production is not a regional anomaly but part of a wider mid-latitude marine response, even as mechanisms and magnitudes vary regionally. This divergent behaviour between anthropogenic and natural aerosol sources observed in both hemispheres implies that near-term climate forcing over marine-influenced regions cannot be interpreted without accounting for evolving ocean–atmosphere and biogeochemical feedbacks, including extremes from wildfires, marine biological blooms and long-range pollution intrusions.

Constraining short-lived climate forcers will therefore require models to represent changing natural aerosol sources and the frequency and intensity of extreme events, supported by sustained, composition-resolved observations at global supersites. Without these constraints, attribution of regional aerosol forcing—and its sign—can be biased.

Methods

Sites. We used decadal-scale (12/2008–05/2019) observations from two WMO-GAW supersites in opposite hemispheres. The Mace Head Atmospheric Research Station (MHD) on Ireland's west coast (53.33°N, 9.90°W) is uniquely positioned to sample clean marine air under westerly flow and episodic polluted continental outflow under easterly conditions (see detailed site descriptions elsewhere[16,17]), and is operated by the University of Galway. The Kennaook/Cape Grim Baseline Air Pollution Station (CGO) is located on Tasmania's northwest coast (40.68°S, 144.69°E) and is operated by Australia's CSIRO and the Bureau of Meteorology.

Measurements. At MHD, we measured non-refractory PM_1 chemical components (organic-aerosol, OA; sulfate, SO_4; nitrate, NO_3; ammonium, NH_4) at MHD using a high-resolution time-of-flight aerosol mass spectrometer (HR-ToF-AMS; Aerodyne Research Inc., Billerica, MA)[41,42] with a standard tungsten vaporiser (650 °C), operated in V-mode, with 10-minute native resolution (Text S1; before aggregating to monthly values using the method described below). We analysed aerosol composition from December 2008 to May 2019, processing the AMS data using SQUIRREL v1.66G for *m/z* calibration and baseline subtraction, and PIKA v1.26G for HR analysis, within Igor Pro 9.02. Nitrate ionisation efficiency, OA, SO_4 and NH_3 relative ionisation efficiencies, as well as air-beam and composition-dependent collection efficiency corrections, followed standard protocols.[43,44,41,45] We calculated methanesulfonic acid (MSA), non-sea-salt SO_4 ($nssSO_4$), and sea-salt (SS) concentrations from the AMS measurements following established approaches (Text S1).[43,46] We estimated ammonium-nitrate (AN) and ammonium-sulfate (AS) salts from the NO_3 and $nssSO_4$ mass-concentrations, respectively (Text S2).

At CGO, we measured MSA and $nssSO_4$ on filters (EMFAB Pallflex Membrane filters) collected using a high-volume sampler (Ecotech 3000) with a PM_{10} size selective inlet. We collected the filters from the marine sector only (using a baseline switch that utilises particle number concentrations and wind direction, as described elsewhere[25]), and determined the concentration

of anions and cations with a Dionex ICS-3000 reagent free ion chromatograph. We calculated $nssSO_4$ from total sulfate concentration and magnesium ion concentration as a conservative tracer for seawater sulfate concentrations.

We measured equivalent black carbon (BC) at MHD at 880 nm[47] using aethalometers (Magee Scientific), specifically model 16 (AE16) until 07/2017, followed by model 33 (AE33)[48] since 12/2017. At CGO, we measured BC using a multi-angle absorption photometer (Thermo-Scientific model 5012).

Environmental parameters: We retrieved for MHD the air temperature (T) and wind speed from the Met Éireann Hourly Data product, accessed via data.gov.ie, and aggregated to monthly means for 2008–2019 to match aerosol trend analysis. We obtained sea surface temperature (SST) from the Copernicus Marine Service Global Ocean OSTIA Level-4 foundation SST analysis (daily, 0.05° grid), extracted at the nearest grid cell to MHD, and aggregated to monthly means over 2008–2019.

Aerosol source speciation. To characterise natural and anthropogenic source contributions to OA, we applied positive matrix factorization (PMF)[49,50] to the MHD HR-ToF-AMS OA mass spectra using the SoFi v6.8.1 toolkit.[51] Factor identification was based on running free PMF on year 2010 spectra at raw 10-minute time resolution (Text S2). The 6 identified factors (Fig. S1) included hydrocarbon-like OA from regional oil/petrol burning (Oil/Petrol-OA), peat-combustion OA (Peat-OA), biomass-burning OA (BBOA), primary marine OA (PMOA), methanesulfonic acid-related OA (MSA-OA), and oxygenated OA (OOA). Factor validation was largely based on spectral matching (cosine similarity) from past work including MHD/Ireland (Text S2). Subsequently, we averaged the entire (decadal) time series of the HR OA mass spectra hourly and subjected the combined matrices to multi-year PMF analysis by constraining the 6 factors identified in the free PMF run using a = 0.1 (Text S2). To differentiate biogenic/natural (marine) and anthropogenic (continental)

contributions to AS (AS_b vs. AS_a) and OOA (OOA_b vs. OOA_a), we applied a criteria-based attribution method (Text S2).

Anthropogenic components effectively respond to emission controls, whereas natural components are largely modulated by meteorology, ocean biogeochemistry and biomass-burning regimes. BBOA at MHD reflects a mixture of regional residential wood burning and gorse/grass fires in surrounding uplands (Text S2), but upper-tail events coincide with wildfire periods; we therefore assign BBOA to the natural group to emphasise climate-sensitive biomass-burning variability. Our anthropogenic–natural split is based on dominant controlling processes rather than a strict natural–versus–anthropogenic ignition dichotomy, and radiative-forcing-related conclusions are insensitive to whether BBOA is classified as natural or anthropogenic.

Decadal trend analysis. For decadal-scale trend analysis, we aggregated hourly resolved concentration data into monthly means; we imputed months with missing data or low coverage using the median of the same calendar month across all years (Text S3) as the analysis requires gapless data. We decomposed the aerosol component-specific (*i*) monthly time series *j* observations ($O_{i,j}$) into additive trend ($T_{i,j}$), seasonal ($S_{i,j}$), and residual ($R_{i,j}$) components using Seasonal-Trend Decomposition via Loess (STL),[14] with 12-month periodicity and parameters optimised to isolate low-frequency trends (Text S3): $O_{i,j} = T_{i,j} + S_{i,j} + R_{i,j}$ (1). STL has been previously used in hydrology,[52,53] epidemiology, and air quality research to examine particulate matter (PM) and trace gas trends.[54,55,56,57,58]

We then applied quantile regression (QR)[15] to $T_{i,j}$ (STL Trends) across quantiles ($\tau = 0.05$–0.95, in 0.05 increments) or $R_{i,j}$ ($\tau = 0.95$). QR estimates the conditional quantile $Q_Y(\tau|t)$ of a response variable Y_j as a function of time, enabling trend analysis across different parts of the distribution. For a given quantile, the model takes the form $Q_Y(\tau|t) = \beta_0(\tau)+\beta_1(\tau)t$ (2),

where $\beta_1(\tau)$ is the slope at quantile τ. Coefficients are estimated by minimising the check loss function $\rho_\tau(u) = u(\tau - I\{u<0\})$, which differentially weights over- and under-predictions. Prior research has employed QR to quantify trends across the entire distribution (i.e. at any chosen quantile) of $PM_{2.5}$ or trace gases,[59,60,61,62,63] enabling explicit evaluation of changes in baseline concentrations, median behaviour, and upper-tail extremes.

We expressed Trend slopes both in absolute (ng m^{-3} yr^{-1}) and relative (% yr^{-1}, using the quantile-specific predicted concentration at median time as baseline) terms. We report 95% confidence intervals for QR slopes. Slopes are statistically significant when the 95% confidence interval excludes zero. We compared QR results for $T_{i,j}$ at τ=0.50 to Theil–Sen regression[64] estimates and ordinary least squares (OLS). Because STL explicitly separates seasonal structure, comparisons involving methods applied directly to raw daily/monthly series (Fig. S6) should be interpreted as sensitivity to preprocessing (seasonality/serial dependence) rather than as fully equivalent trend tests. Finally, we inspected the STL Residuals ($R_{i,j}$) for autocorrelation[65] and corrected them using autoregressive models as needed before obtaining QR results at τ=0.95 (Text S3; Table S1).

From concentration to radiative forcing trends. To estimate decadal-scale direct radiative forcing trends (ΔF_i, in W m^{-2} $decade^{-1}$), we scaled surface concentration changes (ΔC_i, ng m^{-3} yr^{-1}) obtained from QR (at τ=0.25, 0.50, and 0.75) on the STL $T_{i,j}$, to column burdens assuming a mixed layer height (H), then converted to optical depth using component-specific extinction or absorption efficiencies (E_i, in m^2 g^{-1}), and finally multiplied by radiative forcing efficiencies (ε_i, in W m^{-2} per AOD_{550}): $\Delta F_i = \Delta C_i \cdot H \cdot 10^{-9} \cdot E_i \cdot \varepsilon_i$ (3)

A Monte Carlo framework (50,000 iterations) simultaneously sampled uncertainties in ΔC_i, H, E_i, and ε_i (Table S2) to generate probability distributions for component-level, anthropogenic (ΔF_{anthro}), biogenic/natural (ΔF_{nat}), and net forcing trends (Text S4-S5).

Data availability

Raw data that support the findings of this study are available from the corresponding authors upon reasonable request. Data presented in figures will be made publicly available in Zenodo (Moschos, 2026)[66] upon manuscript acceptance.

Code availability

All statistical analyses and visualisations were performed in Python 3.11 using *pandas*, *NumPy*, *SciPy*, and *statsmodels* (time-series decomposition and quantile regression), with *matplotlib* (and *seaborn*) for visualisation. Report generation used *python-docx*. Code to reproduce the STL–QR trend analysis and Monte Carlo forcing calculations will be made publicly available in a GitHub repository upon manuscript acceptance.

References

[1] IPCC, 2021: Climate Change 2021: The Physical Science Basis. Contribution of Working Group I to the Sixth Assessment Report of the Intergovernmental Panel on Climate Change [Masson-Delmotte, V., P. Zhai, A. Pirani, S.L. Connors, C. Péan, S. Berger, N. Caud, Y. Chen, L. Goldfarb, M.I. Gomis, M. Huang, K. Leitzell, E. Lonnoy, J.B.R. Matthews, T.K. Maycock, T. Waterfield, O. Yelekçi, R. Yu, and B. Zhou (eds.)]. Cambridge University Press, Cambridge, United Kingdom and New York, NY, USA, 2391 pp. DOI:10.1017/9781009157896.

[2] Quaas, J.; Jia, H. L.; Smith, C.; Albright, A. L.; Aas, W.; Bellouin, N.; Boucher, O.; Doutriaux-Boucher, M.; Forster, P. M.; Grosvenor, D.; et al. Robust evidence for reversal of the trend in aerosol effective climate forcing. *ACP* **2022**, *22* (18), 12221-12239. DOI: 10.5194/acp-22-12221-2022.

[3] Bellouin, N.; Quaas, J.; Gryspeerdt, E.; Kinne, S.; Stier, P.; Watson-Parris, D.; Boucher, O.; Carslaw, K. S.; Christensen, M.; Daniau, A. L.; et al. Bounding global aerosol radiative forcing of climate change. *Rev Geophys* **2020**, *58* (1), ARTN e2019RG000660. DOI: 10.1029/2019RG000660.

[4] Li, J. W.; Han, Z. W.; Yao, X. H.; Xie, Z. X.; Tan, S. C. The distributions and direct radiative effects of marine aerosols over East Asia in springtime. *STOTEN* **2019**, *651*, 1913-1925. DOI: 10.1016/j.scitotenv.2018.09.368.

[5] Laj, P.; Bigi, A.; Rose, C.; Andrews, E.; Myhre, C. L.; Coen, M. C.; Lin, Y.; Wiedensohler, A.; Schulz, M.; Ogren, J. A.; et al. A global analysis of climate-relevant aerosol properties retrieved from the network of Global Atmosphere Watch (GAW) near-surface observatories. *AMT* **2020**, *13* (8), 4353-4392. DOI: 10.5194/amt-13-4353-2020.

[6] Reddington, C. L.; Carslaw, K. S.; Stier, P.; Schutgens, N.; Coe, H.; Liu, D.; Allan, J.; Browse, J.; Pringle, K. J.; Lee, L. A.; et al. The global aerosol synthesis and science project (GASSP): Measurements and modeling to reduce uncertainty. *BAMS* **2017**, *98* (9), 1857-1877. DOI: 10.1175/Bams-D-15-00317.1.

[7] Jennings, S. G.; Kleefeld, C.; O'Dowd, C. D.; Junker, C.; Spain, T. G.; O'Brien, P.; Roddy, A. F.; O'Connor, T. C. Mace Head Atmospheric Research Station - characterization of aerosol radiative parameters. *Boreal Environ. Res.* **2003**, *8* (4), 303-314.

[8] Zhang, Z.; Li, J.; Che, H.; Dong, Y.; Dubovik, O.; Eck, T.; Gupta, P.; Holben, B.; Kim, J.; Lind, E.; et al. Long-term trends in aerosol properties derived from AERONET measurements. *ACP* **2025**, *25* (8), 4617-4637. DOI: 10.5194/acp-25-4617-2025.

[9] Li, J.; Carlson, B. E.; Lacis, A. A. How well do satellite AOD observations represent the spatial and temporal variability of $PM_{2.5}$ concentration for the United States? *Atmos. Environ.* **2015**, *102*, 260-273. DOI: 10.1016/j.atmosenv.2014.12.010.

[10] Jia, H. L.; Ma, X. Y.; Yu, F. Q.; Quaas, J. Significant underestimation of radiative forcing by aerosol-cloud interactions derived from satellite-based methods. *Nat. Commun.* **2021**, *12* (1), ARTN 4241, DOI: 10.1038/s41467-021-24518-6.

[11] Collaud Coen, M.; Andrews, E.; Bigi, A.; Martucci, G.; Romanens, G.; Vogt, F. P. A.; Vuilleumier, L. Effects of the prewhitening method, the time granularity, and the time segmentation on the Mann–Kendall trend detection and the associated Sen's slope. *AMT* **2020**, *13* (12), 6945-6964. DOI: 10.5194/amt-13-6945-2020.

[12] Burke, M.; Childs, M. L.; de la Cuesta, B.; Qiu, M. H.; Li, J.; Gould, C. F.; Heft-Neal, S.; Wara, M. The contribution of wildfire to $PM_{2.5}$ trends in the USA. *Nature* **2023**, *622* (7984), 761-766. DOI: 10.1038/s41586-023-06522-6.

[13] Chang, K. L.; Schultz, M. G.; Lan, X.; McClure-Begley, A.; Petropavlovskikh, I.; Xu, X. B.; Ziemke, J. R. Trend detection of atmospheric time series: Incorporating appropriate uncertainty estimates and handling extreme events. *Elementa Sci. Anthrop.* **2021**, *9* (1). DOI: 10.1525/elementa.2021.00035.

[14] Cleveland, R.B., Cleveland, W.S. STL: A Seasonal-Trend Decomposition procedure based on Loess. *J. Off. Stat.* **1990**, 6, 3-33.

[15] Koenker, R.; Bassett, G. Regression quantiles. *Econometrica* **1978**, *46* (1), 33-50. DOI: 10.2307/1913643.

[16] O'Connor, T. C.; Jennings, S. G.; O'Dowd, C. D. Highlights of fifty years of atmospheric aerosol research at Mace Head. *Atmos. Res.* **2008**, *90* (2-4), 338-355. DOI: 10.1016/j.atmosres.2008.08.014.

[17] O'Dowd, C.; Ceburnis, D.; Ovadnevaite, J.; Vaishya, A.; Rinaldi, M.; Facchini, M. C. Do anthropogenic, continental or coastal aerosol sources impact on a marine aerosol signature at Mace Head? *ACP* **2014**, *14* (19), 10687-10704. DOI: 10.5194/acp-14-10687-2014.

[18] Grigas, T.; Ovadnevaite, J.; Ceburnis, D.; Moran, E.; McGovern, F. M.; Jennings, S. G.; O'Dowd, C. Sophisticated clean air strategies required to mitigate against particulate organic pollution. *Sci. Rep.* **2017**, *7*, 44737. DOI: 10.1038/srep44737.

[19] Lindgren, S. The coast is clear: Shipping emission standards, air quality and infant health. *TRD* **2021**, *100*, ARTN 103067. DOI: 10.1016/j.trd.2021.103067.

[20] Goodman, P. G.; Rich, D. Q.; Zeka, A.; Clancy, L.; Dockery, D. W. Effect of air pollution controls on black smoke and sulfur dioxide concentrations across Ireland. *JA&WMA* **2009**, *59* (2), 207-213. DOI: 10.3155/1047-3289.59.1.207.

[21] Iizuka, Y.; Matsumoto, M.; Kawakami, K.; Sasage, M.; Ishino, S.; Hattori, S.; Uemura, R.; Matsui, H.; Fujita, K.; Oshima, N.; et al. Acidity-driven gas-particle partitioning of nitrate regulates its transport to Arctic through the industrial era. *Nat. Commun.* **2025**, *16* (1), ARTN 4272. DOI: 10.1038/s41467-025-59208-0.

[22] Shah, V.; Jaeglé, L.; Thornton, J. A.; Lopez-Hilfiker, F. D.; Lee, B. H.; Schroder, J. C.; Campuzano-Jost, P.; Jimenez, J. L.; Guo, H. Y.; Sullivan, A. P.; et al. Chemical feedbacks weaken the wintertime response of particulate sulfate and nitrate to emissions reductions over the eastern United States. *PNAS* **2018**, *115* (32), 8110-8115. DOI: 10.1073/pnas.1803295115.

[23] Kim, H.; Walters, W. W.; Kysela, L.; Hastings, M. G. Long-term trends in inorganic aerosol chemical composition and chemistry at an urban and rural site in the northeastern US. *STOTEN* **2023**, *904*, ARTN 166848. DOI: 10.1016/j.scitotenv.2023.166848.

[24] Li, M. M.; Zhang, Z. H.; Yao, Q.; Wang, T. J.; Xie, M.; Li, S.; Zhuang, B. L.; Han, Y. Nonlinear responses of particulate nitrate to NO_x emission controls in the megalopolises of China. *ACP* **2021**, *21* (19), 15135-15152. DOI: 10.5194/acp-21-15135-2021.

[25] Gras, J. L.; Keywood, M. Cloud condensation nuclei over the Southern Ocean: wind dependence and seasonal cycles. *ACP* **2017**, *17* (7), 4419-4432. DOI: 10.5194/acp-17-4419-2017.

[26] Xu, W.; Ovadnevaite, J.; Fossum, K. N.; Lin, C. S.; Huang, R. J.; Ceburnis, D.; O'Dowd, C. Sea spray as an obscured source for marine cloud nuclei. *Nat. Geosci.* **2022**, *15* (4), 282-286. DOI: 10.1038/s41561-022-00917-2.

[27] Zhai, D. R.; Beaulieu, C.; Kudela, R. M. Long-term trends in the distribution of ocean chlorophyll. *GRL* **2024**, *51* (7), ARTN e2023GL106577. DOI: 10.1029/2023GL106577.

[28] Laing, J. R.; Hopke, P. K.; Hopke, E. F.; Husain, L.; Dutkiewicz, V. A.; Paatero, J.; Viisanen, Y. Long-term trends of biogenic sulfur aerosol and its relationship with sea surface temperature in Arctic Finland. *JGR Atmos.* **2013**, *118* (20), 11770-11776, Artn 776. DOI: 10.1002/2013jd020384.

[29] Flores, J. M.; Bourdin, G.; Kostinski, A. B.; Altaratz, O.; Dagan, G.; Lombard, F.; Haëntjens, N.; Boss, E.; Sullivan, M. B.; Gorsky, G.; et al. Diel cycle of sea spray aerosol concentration. *Nat. Commun.* **2021**, *12* (1), ARTN 5476. DOI: 10.1038/s41467-021-25579-3.

[30] Hu, J.; Li, J. L.; Tchinda, N. T.; Song, Y. R.; Xu, M. L.; Li, K.; Du, L. Underestimated role of sea surface temperature in sea spray aerosol formation and climate effects. *Npj Clim. Atmos. Sci.* **2024**, *7* (1), ARTN 273. DOI: 10.1038/s41612-024-00823-x.

[31] Ribeiro, C. B.; Will, R.; Tibúrcio, I. V. R.; Borth, R. C.; Hoinaski, L. Global trends and drivers of black carbon in the atmosphere. *Environ. Technol.* **2025**, 1–14. DOI: 10.1080/09593330.2025.2528329.

[32] Simó, R.; Dachs, J. Global ocean emission of dimethylsulfide predicted from biogeophysical data. *Glob. Biogeochem. Cycle.* **2002**, *16* (4), Artn 1078. DOI: 10.1029/2001gb001829.

[33] Golder, M. R.; Antoine, D. Physical drivers of long-term chlorophyll-a variability in the Southern Ocean. *Elementa Sci. Anthrop.* **2025**, *13* (1), ARTN 00077. DOI: 10.1525/elementa.2024.00077.

[34] Spokes, L. J.; Yeatman, S. G.; Cornell, S. E.; Jickells, T. D. Nitrogen deposition to the eastern Atlantic Ocean. The importance of south-easterly flow. *Tellus B.* **2000**, *52* (1), 37-49. DOI: 10.1034/j.1600-0889.2000.00062.x.

[35] Lin, C. S.; Ceburnis, D.; Huang, R. J.; Xu, W.; Spohn, T.; Martin, D.; Buckley, P.; Wenger, J.; Hellebust, S.; Rinaldi, M.; et al. Wintertime aerosol dominated by solid-fuel-burning emissions across Ireland: insight into the spatial and chemical variation in submicron aerosol. *ACP* **2019**, *19* (22), 14091-14106. DOI: 10.5194/acp-19-14091-2019.

[36] Cawkwell, Fiona, Emma Chalençon, Ned Dwyer, Clara Felberbauer, Stig Hellebust, Beatriz Martin, Thedmer Postma, Guy Serbin, and Dean Venables. 2025. *Quantification of the Area of Land Burned and Habitats Affected by Wildfires in Ireland, 2015–2021, and the Resulting Emissions*. EPA Research Report No. 476. Environmental Protection Agency (Ireland).

[37] Scott, C. E.; Arnold, S. R.; Monks, S. A.; Asmi, A.; Paasonen, P.; Spracklen, D. V. Substantial large-scale feedbacks between natural aerosols and climate. *Nat. Geosci.* **2018**, *11* (1), 44-48. DOI: 10.1038/s41561-017-0020-5.

[38] Hodnebrog, O.; Myhre, G.; Jouan, C.; Andrews, T.; Forster, P. M.; Jia, H. L.; Loeb, N. G.; Olivie, D. J. L.; Paynter, D.; Quaas, J.; et al. Recent reductions in aerosol emissions have increased Earth's energy imbalance. *Commun. Earth Environ.* **2024**, *5* (1). DOI: 10.1038/s43247-024-01324-8.

[39] Persad, G.; Samset, B. H.; Wilcox, L. J.; Allen, R. J.; Bollasina, M. A.; Booth, B. B.; Bonfils, C.; Crocker, T.; Joshi, M.; Lund, M. T.; et al. Rapidly evolving aerosol emissions are a dangerous omission from near-term climate risk assessments. *Environ. Res. Clim.* **2023**, *2* (3), ARTN 032001. DOI: 10.1088/2752-5295/acd6af.

[40] Cui, C.; Tian, P. F.; Wang, W. F.; Yu, Z. R.; Wang, B. R.; Tang, C. G.; Cao, X. J.; Liang, J. N.; Zhang, L. Increasing coarse aerosols mitigated the warming effect of anthropogenic fine particle reductions in Europe. *Earths Future* **2025**, *13* (4), ARTN e2025EF006044. DOI: 10.1029/2025EF006044.

[41] Canagaratna, M. R.; Jayne, J. T.; Jimenez, J. L.; Allan, J. D.; Alfarra, M. R.; Zhang, Q.; Onasch, T. B.; Drewnick, F.; Coe, H.; Middlebrook, A.; et al. Chemical and microphysical characterization of ambient aerosols with the Aerodyne aerosol mass spectrometer. *Mass Spectrom. Rev.* **2007**, *26* (2), 185-222. DOI: 10.1002/mas.20115.

[42] DeCarlo, P. F.; Kimmel, J. R.; Trimborn, A.; Northway, M. J.; Jayne, J. T.; Aiken, A. C.; Gonin, M.; Fuhrer, K.; Horvath, T.; Docherty, K. S.; et al. Field-deployable, high-resolution, time-of-flight aerosol mass spectrometer. *Anal. Chem.* **2006**, *78* (24), 8281-8289. DOI: 10.1021/ac061249n.

[43] Ovadnevaite, J.; Ceburnis, D.; Leinert, S.; Dall'Osto, M.; Canagaratna, M.; O'Doherty, S.; Berresheim, H.; O'Dowd, C. Submicron NE Atlantic marine aerosol chemical composition and abundance: Seasonal trends and air mass categorization. *JGR Atmos.* **2014**, *119* (20), 11,850-811,863. DOI: 10.1002/2013jd021330.

[44] Middlebrook, A. M.; Bahreini, R.; Jimenez, J. L.; Canagaratna, M. R. Evaluation of composition-dependent collection efficiencies for the Aerodyne aerosol mass spectrometer using field data. *Aerosol Sci. Tech.* **2012**, *46* (3), 258-271. DOI: 10.1080/02786826.2011.620041.

[45] Nault, B. A.; Croteau, P.; Jayne, J.; Williams, A.; Williams, L.; Worsnop, D.; Katz, E. F.; DeCarlo, P. F.; Canagaratna, M. Laboratory evaluation of organic aerosol relative ionization efficiencies in the aerodyne aerosol mass spectrometer and aerosol chemical speciation monitor. *Aerosol Sci. Tech.* **2023**, *57* (10), 981-997. DOI: 10.1080/02786826.2023.2223249.

[46] Ovadnevaite, J.; Ceburnis, D.; Canagaratna, M.; Berresheim, H.; Bialek, J.; Martucci, G.; Worsnop, D. R.; O'Dowd, C. On the effect of wind speed on submicron sea salt mass concentrations and source fluxes. *JGR Atmos.* **2012**, *117*. DOI: 10.1029/2011jd017379.

[47] Petzold, A.; Ogren, J. A.; Fiebig, M.; Laj, P.; Li, S. M.; Baltensperger, U.; Holzer-Popp, T.; Kinne, S.; Pappalardo, G.; Sugimoto, N.; et al. Recommendations for reporting "black carbon" measurements. *ACP* **2013**, *13* (16), 8365-8379. DOI: 10.5194/acp-13-8365-2013.

[48] Drinovec, L.; Mocnik, G.; Zotter, P.; Prévôt, A. S. H.; Ruckstuhl, C.; Coz, E.; Rupakheti, M.; Sciare, J.; Müller, T.; Wiedensohler, A.; et al. The "dual-spot" Aethalometer: an improved measurement of aerosol black carbon with real-time loading compensation. *AMT* **2015**, *8* (5), 1965-1979. DOI: 10.5194/amt-8-1965-2015.

[49] Paatero, P.; Tapper, U. Positive Matrix Factorization - a nonnegative factor model with optimal utilization of error-estimates of data values. *Environmetrics* **1994**, *5* (2), 111-126. DOI: 10.1002/env.3170050203.

[50] Paatero, P. The multilinear engine — A table-driven, least squares program for solving multilinear problems, including the n-way parallel factor analysis model. *J. Comput. Graph. Stat.* **1999**, *8* (4), 854-888. DOI: 10.2307/1390831.

[51] Canonaco, F.; Crippa, M.; Slowik, J. G.; Baltensperger, U.; Prévôt, A. S. H. SoFi, an IGOR-based interface for the efficient use of the generalized multilinear engine (ME-2) for the source apportionment: ME-2 application to aerosol mass spectrometer data. *AMT* **2013**, *6* (12), 3649-3661. DOI: 10.5194/amt-6-3649-2013.

[52] Sellinger, C. E.; Stow, C. A.; Lamon, E. C.; Qian, S. S. Recent water level declines in the Lake Michigan-Huron system. *Environ. Sci. Technol.* **2008**, *42* (2), 367-373. DOI: 10.1021/es070664.

[53] Stow, C. A.; Cha, Y.; Johnson, L. T.; Confesor, R.; Richards, R. P. Long-term and seasonal trend decomposition of Maumee River nutrient inputs to western Lake Erie. *Environ. Sci. Technol.* **2015**, *49* (6), 3392-3400. DOI: 10.1021/es5062648.

[54] Borchers-Arriagada, N.; Vander Hoorn, S.; Cope, M.; Morgan, G.; Hanigan, I.; Williamson, G.; Johnston, F. H. The mortality burden attributable to wood heater smoke particulate matter ($PM_{2.5}$) in Australia. *STOTEN* **2024**, *921*. DOI: 10.1016/j.scitotenv.2024.171069.

[55] Chen, Y.; Rich, D. Q.; Masiol, M.; Hopke, P. K. Changes in ambient air pollutants in New York State from 2005 to 2019: Effects of policy implementations and economic and technological changes. *Atmos. Environ.* **2023**, *311*. DOI: 10.1016/j.atmosenv.2023.119996.

[56] Carslaw, D. C. On the changing seasonal cycles and trends of ozone at Mace Head, Ireland. *ACP* **2005**, *5*, 3441-3450. DOI: DOI 10.5194/acp-5-3441-2005.

[57] Chaloupka, M. Historical trends, seasonality and spatial synchrony in green sea turtle egg production. *Biol. Conserv.* **2001**, *101* (3), 263-279. DOI: 10.1016/S0006-3207(00)00199-3.

[58] Hafen, R. P.; Anderson, D. E.; Cleveland, W. S.; Maciejewski, R.; Ebert, D. S.; Abusalah, A.; Yakout, M.; Ouzzani, M.; Grannis, S. J. Syndromic surveillance: STL for modeling, visualizing, and monitoring disease counts. *Bmc. Med. Inform. Decis.* **2009**, *9*. DOI: 10.1186/1472-6947-9-21.

[59] Porter, W. C.; Heald, C. L.; Cooley, D.; Russell, B. Investigating the observed sensitivities of air-quality extremes to meteorological drivers via quantile regression. *ACP* **2015**, *15* (18), 10349-10366. DOI: 10.5194/acp-15-10349-2015.

[60] McClure, C. D.; Jaffe, D. A. Investigation of high ozone events due to wildfire smoke in an urban area. *Atmos. Environ.* **2018**, *194*, 146-157. DOI: 10.1016/j.atmosenv.2018.09.021.

[61] Barmpadimos, I.; Keller, J.; Oderbolz, D.; Hueglin, C.; Prévôt, A. S. H. One decade of parallel fine ($PM_{2.5}$) and coarse (PM_{10}–$PM_{2.5}$) particulate matter measurements in Europe: trends and variability. *ACP* **2012**, *12* (7), 3189-3203. DOI: 10.5194/acp-12-3189-2012.

[62] Sayegh, A. S.; Munir, S.; Habeebullah, T. M. Comparing the performance of statistical models for predicting PM concentrations. *AAQR* **2014**, *14* (3), 653-665. DOI: 10.4209/aaqr.2013.07.0259.

[63] Seguel, R. J.; Castillo, L.; Opazo, C.; Rojas, N. Y.; Nogueira, T.; Cazorla, M.; Gavidia-Calderón, M.; Gallardo, L.; Garreaud, R.; Carrasco-Escaff, T.; et al. Changes in South American surface ozone trends: exploring the influences of precursors and extreme events. *ACP* **2024**, *24* (14), 8225-8242. DOI: 10.5194/acp-24-8225-2024.

[64] Sen, P. K. Estimates of regression coefficient based on Kendall's tau. *J. Am. Stat. Assoc.* **1968**, *63* (324), 1379–1389.

[65] Ljung, G. M.; Box, G. E. P. Measure of lack of fit in time-series models. *Biometrika* **1978**, *65* (2), 297-303. DOI: 10.2307/2335207.

[66] Moschos, V. (2026). Rising natural aerosols drive marine radiative forcing as pollution declines [Data set]. Zenodo. DOI: 10.5281/zenodo.18436704, last access: 30 January 2026.

Acknowledgements

This work was supported by the EPA Research Programme 2021-2030, a Government of Ireland initiative funded by the Department of Climate, Energy and the Environment, under project AEROTREND (grant no. 2025-CE-1342); and Taighde Éireann – Research Ireland (grant no. 22/FFP-A/10611). JBP was supported by the Australian Research Council Discovery Project: DP240100389, obtained by Branka Miljevic. We thank Zoran Ristovski and Branka Miljevic for fruitful discussions; Liz Coleman for insightful feedback; Sally Taylor, Paul Selleck, and Jennifer Powell for CGO filter analysis; and Jason Ward, Jeremy Ward, Nigel Somerville, Jennifer Powell, and Fabienne Reisen for CGO filter collection and BC data collection. The Australian Bureau of Meteorology and CSIRO are acknowledged for their ongoing support of the Kennaook/Cape Grim Station.

Author contributions

VM: conceptualization, data curation, formal analysis, funding acquisition, investigation, methodology, project administration, software, validation, visualisation, and writing – original draft; COD: resources; DC: data curation, and investigation; JO: conceptualization, data curation, funding acquisition, and investigation. Review & Editing: all co-authors.

Competing interests statement

The authors declare no competing interests.

Supplementary information

Figures S1–S7, Tables S1–S2, Supplementary Text S1–S5, and SI References.

Supplementary Files

This is a list of supplementary files associated with this preprint. Click to download.

- MoschosetalSI.pdf